The Meteoritical Society

Meteoritics & Planetary Science 48, Nr 12, 2480–2490 (2013)
doi: 10.1111/maps.12233

I-Xe ages of Campo del Cielo silicates as a record of the complex early history of the IAB parent body

O. PRAVDIVTSEVA[1*], A. MESHIK[1], C. M. HOHENBERG[1], and G. KURAT[2†]

[1]McDonnell Center for the Space Sciences and Physics Department of Washington University, One Brookings Drive, Saint Louis, Missouri 63130, USA
[2]Department of Lithospheric Sciences, University of Vienna, Althanstrasse 14, Vienna 1090, Austria
[†]Deceased
[*]Corresponding author. E-mail: olga@physics.wustl.edu

(Received 27 November 2012; revision accepted 09 October 2013)

Abstract–Using in situ laser analyses of a polished thin section from the IAB iron meteorite Campo del Cielo, we identified two silicate grains rich in radiogenic ^{129*}Xe, Cr-diopside, and oligoclase, excavated them from the metal, and irradiated them with thermal neutrons for I-Xe dating. The release profiles of ^{129*}Xe and ^{128*}Xe are consistent with these silicates being diopside and oligoclase, with activation energies, estimated using Arrhenius plots, of ~201 and ~171 kcal mole^{-1}, respectively. The 4556.4 ± 0.4 Ma absolute I-Xe age of the more refractory diopside is *younger* than the 4558.0 ± 0.7 Ma I-Xe age of the less refractory oligoclase. We suggest that separate impact events at different locations and depths on a porous initial chondritic IAB parent body led to the removal of the melt and recrystallization of diopside and oligoclase at the times reflected by their respective I-Xe ages. The diopside and oligoclase grains were later brought into the studied inclusion by a larger scale catastrophic collision that caused breakup and reassembly of the debris, but did not reset the I-Xe ages dating the first events. The metal melt most probably was <1250 °C when it surrounded studied silicate grains. This reassembly could not have occurred earlier than the I-Xe closure in diopside at 4556.4 ± 0.4 Ma.

INTRODUCTION

IAB iron meteorites are an intriguing nonmagmatic group with complex characteristics that do not fit into any simple formation scenario. They contain chondritic silicates closely related to carbonaceous chondrites with plagioclase contents that vary from clast to clast. Iridium fractionation in IAB irons is minor compared with the iron meteorites that formed by fractional crystallization, small γ crystals indicate rapid cooling through the γ-iron stability field. Although it is generally agreed that the formational and thermal history of the IAB parent body is related to metal-silicate fractionation in the interior of planetesimals or planets, there is an ongoing discussion on whether the triggers for this fractionation are internal heat sources (Kelly and Larimer 1977; Kracher 1982, 1985), external heat sources such as impacts (Wasson et al. 1980; Choy et al. 1995; Wasson and Kallemeyn 2002), or both (Benedix et al. 2000; Takeda et al. 2000).

IAB silicates are known to contain abundant primordial noble gases and Ar-Ar and I-Xe ages have been measured in various separated mineral phases from these meteorites in attempts to gain insight into the early thermal history of the IAB parent body. The I-Xe system is expected to be the more retentive one and the reported I-Xe ages for IAB silicates are indeed consistently older than the Ar-Ar ages for the same meteorites (Podosek 1970; Niemeyer 1979a, 1979b; Takeda et al. 2000; Bogard et al. 2005; Vogel and Renne 2008; Pravdivtseva et al. 2009). The I-Xe age of Mundrabilla troilite (Niemeyer 1979a) even seemed to predate the formation of CAIs at 4567.30 ± 0.16 Ma (Amelin et al. 2002, 2010; Connelly et al. 2012), initially casting some doubt on the validity of the I-Xe chronometer itself until it was discovered that this anomalous age was due to faulty I-Xe monitors

(Hohenberg et al. 1981). Calculated relative to the reproducible Shallowater standard as a monitor (Gilmour et al. 2009), the later obtained I-Xe ages of silicates from IAB iron meteorites provided results consistent with early solar system chronology (Pravdivtseva et al. 2000; Bogard et al. 2005). The I-Xe system in single pyroxene grains from a Toluca IAB silicate/graphite nodule provided closure times for high- and low-Mg pyroxenes and the means to estimate the cooling rate at the time of exsolution (Pravdivtseva et al. 2009). As single grains with known mineralogy are simple systems with well-defined thermal properties, I-Xe studies of individual grains can often reveal new details of the parent body evolution, such as the cooling rates inferred for Toluca. We took this same approach for Campo del Cielo in an attempt to obtain additional information on the complex early history of IAB iron meteorites that may still be reflected in the I-Xe system of its silicates.

In this paper, we present the I-Xe data for two single silicate grains from a Campo del Cielo silicate-graphite-metal (SiGrMet) inclusion (collection of the Museum of Natural History in Vienna). Campo del Cielo has been extensively studied since the end of the 18th century, with first results from noble gases isotopic analyses published in 1960-th (Alexander and Manuel 1968; Hintenberger et al. 1968; Alexander et al. 1969). One early study of noble gases from Campo del Cielo (Hintenberger et al. 1968) was performed on two inclusions recovered from a large piece freshly cut from the 1993.8 kg slab of Campo del Cielo referred to as El Taco, a name often erroneously given to the meteorite itself. Besides a variable amount of graphite, these inclusions contained plagioclase, enstatite, diopside, and olivine. The inclusions were crushed, sieved, and a portion of the grain-size fraction 0.2–0.1 mm was chemically treated in HBr to obtain a pure silicate phase, free of iron and troilite. Stepwise heating analyses of this silicate fraction revealed a maximum $^{129}Xe/^{132}Xe$ ratio of 3.85, approximately 4 times higher than the atmospheric value. In 1970, Podosek reported an I-Xe age for a Campo del Cielo silicate inclusion which, when calibrated to the absolute age of Shallowater, yielded an age of 4559.9 ± 0.7 Ma. This inclusion weighed 1.4 g and consisted of many different types of silicates, so the I-Xe age was a composite not associated with any single mineral phase (Podosek 1970). We overcome this limitation by studying single mineral grains with unique thermal properties. It was reported that Campo del Cielo shows highly variable degrees of low-temperature plagioclase-rich melt losses not only between different silicate inclusions but also within single inclusions (Wlotzka and Jarosewich 1977). Our work was intended to investigate if these mineralogical variations are reflected in xenon isotopic compositions and in the I-Xe ages of single grains separated from the same SiGrMet inclusion.

EXPERIMENTAL PROCEDURE

From a large (approximately 10 cm) round SiGrMet inclusion from Campo del Cielo, which consists mainly of granular metal with variable amounts of silicates dispersed throughout, we prepared a polished section for mineral identification and in situ Xe analyses. This specimen contains abundant millimeter-sized silicates, commonly enveloped by graphite (Fig. 1a).

The minerals were identified by optical and analytical electron microscopy, utilizing a JEOL-840A scanning microscope. As the silicates were of primary interest in these studies, we acquired X-ray spectra of numerous silicate inclusions. The majority of these cluster together in composition, belonging to the plagioclase feldspar series with elemental compositions consistent with oligoclase ($Al_{15–20}An_{85–80}$). Single bright green chromium diopside grains are uniformly dispersed throughout the polished section and olivines are rare.

To identify possible iodine carrier phases, we measured Xe isotopic compositions and abundances in silicates and in the metal by in situ laser extraction, using an acoustically Q-switched Nd-YAG laser (1064 nm). Graphite rims enveloping the silicates are mostly 7–10 μm in thickness, smaller than the laser spot size, and are not wide enough for unique laser in situ analyses. After rastering a 300 × 300 μm area, which takes about 40 s with an average laser power of 25 W and 25 μm spot size, the cell was opened to the sample system for another 50 s, transferring the gas, and then closed for cleanup. In this way, the bulk of the extracted gas was isolated from the extraction system, a procedure which allowed us to reach a ^{132}Xe blank of less than 5×10^{-15} cm^3 STP, while losing only about 5% of the extracted Xe. Released gases were cleaned sequentially by first exposing them to SAES St707 getter pellets, maintained at 275 °C, and then to freshly deposited Ti-film getters. The heavy noble gases were separated from He, Ne, and Ar using activated charcoal at a temperature of −90 °C for adsorption of the Xe (the light gases were pumped away) and +165 °C for Xe desorption. The isotopic composition of the released Xe was measured by high transmission ion-counting mass-spectrometry (Hohenberg 1980).

Eight different 300 × 300 μm areas were rastered, each approximately 12 μm deep with typical rasters shown in Figs. 1(b) and 1(c). The resulting concentrations of radiogenic $^{129*}Xe$ are given in Table 1. The concentration values are probably overestimated due to the heating and possible degasing of the areas surrounding excavated holes. However, they clearly indicate excesses of

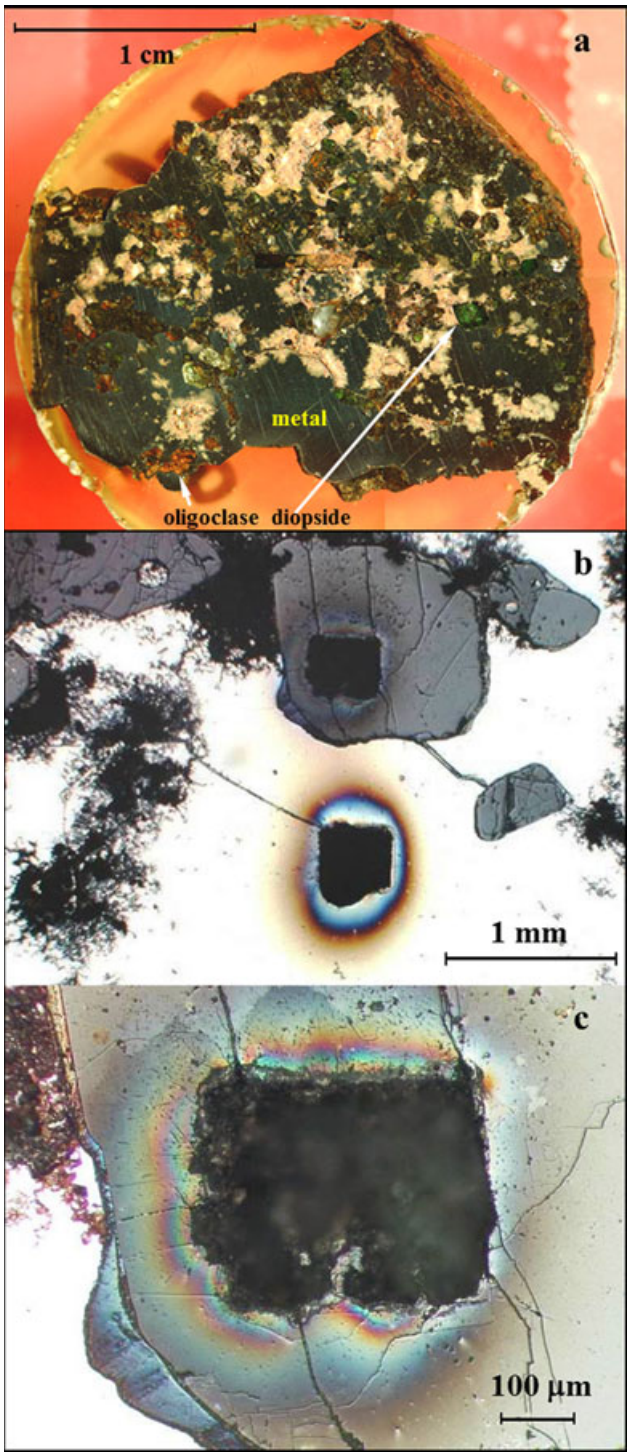

Fig. 1. a) Polished section of Campo del Cielo embedded in epoxy. b) Laser excavated 300 × 300 µm areas of Campo del Cielo iron. 1—diopside, 2—metal. Rust lace is visible at the left. c) Excavated area of diopside grain, hairline fractures formed after laser rastering, graphite rim is visible to the left.

radiogenic ^{129*}Xe in both diopside and oligoclase. In fact, the released Xe was almost monoisotopic ^{129*}Xe with no measurable amount of trapped Xe. There was no detectable fission Xe in either mineral. No radiogenic ^{129*}Xe was observed in the metal itself, nor was it found in the rust or in olivine.

Table 1. Concentrations of radiogenic ^{129*}Xe in various grains from SiGrMet inclusion of Campo del Cielo (estimated to be approximately 15% uncertain).

Rastered mineral	^{129*}Xe × 10^{-7} cm^3 STP g^{-1}
Diopside (#1)	4.5
Diopside (#3)	5.4
Oligoclase without Fe (#6)	0.9
Oligoclase with Fe (#8)	5.6
Olivine (#4)	<0.01
Rusty spot (#2)	<0.02
Metal (#7)	<0.04
Metal (#5)	<0.03

Although diopside #3 had a slightly higher concentration of radiogenic ^{129*}Xe, diopside #1 was larger and did not have any visible microinclusions. It was surrounded mostly by metal and separated from the single adjacent silicate by a graphite rim (Fig. 1b), so we selected that specimen for irradiation and further I-Xe studies. Diopside #1 was manually excavated from the metal matrix with a stainless steel needle as a single 2.15 mg crystal. Plagioclase veins consisted of agglomerates of smaller inclusions, characterized by varying Fe content. Plagioclase, containing the rastered area #8, was brittle and was recovered from the metal matrix in three pieces with a combined weight of 0.18 mg. The selected silicates were rinsed in methanol, dried, and sealed individually under vacuum in fused quartz ampoules.

Samples, along with the Shallowater enstatite irradiation standard, were irradiated with thermal neutrons as part of the SLC–16 capsule in the pool area of the Missouri University Research Reactor (MURR), receiving ≈ 2 × 10^{19} n cm^{-2}. The samples were placed in a fixed horizontal plane at the center of the vertical neutron profile in the pool of the reactor to minimize any vertical gradient and the capsule was continuously rotated to eliminate any x–y gradient. To monitor the neutron density during the irradiation, four pieces of Co-doped Al monitor wire were placed among the samples in the middle and around the perimeter of the irradiation capsule. After cooling, samples were removed from the quartz ampoules, wrapped in platinum foil, and placed in the extraction system of the mass-spectrometer.

Xenon was released in stepwise extractions in a W-coil, purified according to the earlier described protocol for the laser extraction analyses, and its isotopic composition was measured. Hot blanks were measured with an empty coil at 1500 °C (15 min) following standard analytical procedures and were about 2 × 10^{-15} ^{132}Xe cm^3 STP and approximately atmospheric in

composition. We do not measure extraction temperatures directly during the analysis, but determine them indirectly via the heating coil current. The heating coil temperature as a function of heating coil current was calibrated using an optical pyrometer, and the double-walled radiation shield around the heating coil ensures good agreement between actual extraction temperatures within the coil and the coil temperatures established by the calibration. However, as the coil ages and gets thinner, the resistance goes up, so the power delivered (hence temperature) at a given current goes up. As the samples are routinely wrapped in platinum foil for the analyses, the heating coil current, recorded for each studied sample at the melting of platinum, provides an independent internal calibration. Based on the coil current values, both samples studied here melted at about 50 °C lower than the Pt melting point of 1772 °C. Moreover, 70% of the radiogenic gases for Campo del Cielo diopside were released in a single extraction step at 1350 °C (releasing gases for the 1300–1350 °C interval), an apparent temperature that is about 50 °C lower than the melting temperature of diopside, 1395 °C (Lodders and Fegley 1998). This suggests that the coil current indicates a temperature 50 °C too low, which has been taken into account for the temperature values given here. After the stepwise heating analysis of each sample, the coil was kept for 10 min at a temperature higher than the platinum melting temperature (approximately 2000 °C), and a new hot blank was measured at 1500 °C before analyzing a new sample to ensure that no sample memory effects exist.

RESULTS

The measured Xe isotopic compositions for Campo del Cielo diopside and oligoclase grains and the Shallowater standard are shown in Table 2. Usually, the first temperature extractions during stepwise heating experiments are dominated by uncorrelated ^{128}Xe, indicating superficial iodine contamination. In the case of the Campo del Cielo silicates studied here, only small amounts of uncorrelated ^{128}Xe are present. The isotopic composition of Xe in the first extraction step of diopside, 650 °C, was consistent with air. The 850 °C release contained only 1.9% of the total ^{128}Xe, with 94% of the radiogenic ^{128*}Xe and ^{129*}Xe being released in the temperature range 1250–1400 °C, and 70% of the radiogenic gases were released in a single extraction step at 1350–1400 °C that coincided with the melting point of diopside at 1395 °C (Lodders and Fegley 1998). The I-Xe isochron for diopside (Fig. 2) is defined by nine successive temperature steps, providing an age 5.9 ± 0.2 Ma younger than the Shallowater internal standard, which has an age of 4562.3 ± 0.4 Ma (Gilmour et al. 2009). The absolute age of diopside therefore is 4556.4 ± 0.4 Ma.

Albite ($NaAlSi_3O_8$) and anorthite ($CaAl_2Si_2O_8$) are completely miscible and together form an isomorphous series ranging from the pure soda feldspar (albite) at one end to the pure lime feldspar (anorthite) at the other end of the series. Melting temperatures for this series cover a wide range from 1118 °C for albite to 1557 °C for anorthite (Lodders and Fegley 1998). Compositions of plagioclase between these two endmembers melt or crystallize in a more complex way, as partial crystallization of the endmembers occurs over a range of temperatures. This might be the explanation of the broader release profile of radiogenic ^{128*}Xe and ^{129*}Xe in Campo del Cielo oligoclase compared with diopside (Fig. 3). If the 1300–1350 °C temperature extraction step for oligoclase represents the upper limit of the apparent melting temperature interval, the range of melting temperatures for this silicate inclusion will be about 1160–1350 °C, consistent with the oligoclase X-ray spectra we obtained. The isochron, defined by seven successive experimental points, corresponds to an I-Xe age 4.3 ± 0.6 Ma younger than Shallowater and an absolute age of 4558.0 ± 0.7 Ma. Although melting temperatures are not equal to crystallization temperatures, the ratio of the temperature at which crystallization rate is maximum to the melting temperature is nearly constant for many types of material. As both analyzed samples are silicates, the difference in their melting temperatures will be approximately equal to the difference in their crystallization temperatures and hence to the I-Xe system closure temperatures (Norimasa 1990).

Diopside contained 5.8×10^{-9} cm^3 STP g^{-1} of ^{129*}Xe, the highest concentration observed so far in any of the analyzed IAB silicates. Oligoclase has a concen- tration that is one order of magnitude lower, 5.0×10^{-10} cm^3 STP g^{-1} of ^{129*}Xe. Contrary to earlier observations (Mathew and Begemann 1995), trapped Xe in these silicates is isotopically consistent with the ordinary chondrite (OC) component. Concentrations of ^{132}Xe (after correction for small fission contributions) are 1.4×10^{-10} cm^3 STP g^{-1} and 1.0×10^{-10} cm^3 STP g^{-1}, respectively, some three to five times less than in previously studied silicates from IAB irons (Podosek 1970; Mathew and Begemann 1995). The virtual absence of trapped Xe in the minerals studied here suggests that the trapped gases may be concentrated in the graphite inclusions or graphite rims—similar to what was found by Maruoka et al. (2001) and Matsuda et al. (2005). Maruoka et al. (2001) reported a ^{132}Xe concentration in Bohumilitz (IAB) nonetched graphite to be 42.74×10^{-10} cm^3 STP g^{-1}, compatible with the "El Taco" xenon values in graphite of $(10.54–26.15) \times 10^{-10}$ cm^3 STP g^{-1} observed by Mathew and Begemann (1995). Unfortunately, in most cases, the thickness of the graphite rims around silicate grains in this Campo del Cielo section varies between 7 and 10 μm, making an in situ analysis of the graphite rims currently impossible.

Table 2. Raw I-Xe data for the Shallowater standard and Campo del Cielo silicates.

T, °C	$^{132}Xe \times 10^{-12}$. cm^3 STP g^{-1}	$^{132}Xe \equiv 100$							
		^{124}Xe	^{126}Xe	^{128}Xe	^{129}Xe	^{130}Xe	^{131}Xe	^{134}Xe	^{136}Xe
Shallowater, 37.0 mg									
800	43.86	0.506	0.586	119	117.53	15.92	103.25	42.67	38.25
		0.025	0.02	2.1	0.55	0.09	0.45	0.25	0.23
1000	21.14	0.467	0.428	153.4	123.28	15.95	97.8	41.04	36.27
		0.027	0.034	1.5	0.6	0.15	0.36	0.27	0.25
1100	23.48	0.479	0.443	82	107.31	16.01	93.5	39.38	33.75
		0.019	0.018	0.66	0.54	0.14	0.34	0.28	0.2
1200	62.45	0.455	0.43	36.58	108.47	16.17	107.42	38.48	32.81
		0.016	0.014	0.19	0.4	0.1	0.35	0.13	0.2
1250	28.77	0.472	0.415	28.25	112.19	16.04	114	38.59	32.77
		0.023	0.021	0.21	0.53	0.12	0.5	0.3	0.22
1300	24.46	0.496	0.451	47.63	126.03	16.1	167.78	39.46	33.44
		0.018	0.021	0.29	0.55	0.14	0.57	0.24	0.28
1350	38.51	0.463	0.45	1311.4	966.9	16.6	139.99	39.32	34.19
		0.019	0.024	6	3.6	0.11	0.47	0.24	0.23
1400	58.94	0.441	0.417	73.37	145.55	16.13	90.15	38.43	33.08
		0.017	0.012	0.37	0.53	0.1	0.3	0.15	0.2
1450	2.48	0.479	0.558	539.1	450.5	14.91	104.36	44.21	42.39
		0.086	0.065	3.5	3.2	0.5	1.16	1.07	0.87
1500	0.41	0.252	0.302	510.4	409.1	16.14	106.97	44.51	42.77
		0.202	0.133	8.8	7.6	1.04	3.91	1.84	1.77
1550	0.49	0.371	0.443	855.3	662.3	15.35	119.71	48.81	54.9
		0.167	0.156	12.3	10.5	1.08	3.39	1.24	1.59
1600	0.29	0.391	0.127	38.2	114.1	15.01	79.32	36.6	31.79
		0.226	0.197	2.9	5.1	1.2	3.61	1.73	1.92
1800	6.5	0.317	0.341	75.81	141.6	14.7	82.09	40.23	35.99
		0.044	0.037	0.53	1.1	0.19	0.57	0.22	0.46
Total	311.78	0.465	0.452	230.8	230.1	16.1	110.67	39.6	34.34
		0.007	0.007	1.5	1.4	0.04	0.17	0.08	0.09
Campo del Cielo diopside, 2.15 mg									
600	0.8	−0.04	2.14	13.7	117.1	12.6	103.4	46.7	36
		0.77	0.8	3.1	8.1	2.4	8.6	3.6	5.5
800	9.58	0.51	0.38	2176	893	18.2	180.7	40.3	36.1
		0.16	0.17	31	18	1	5.1	1.7	1.3
900	3.76	0.72	0.23	839	491	15.8	95	34.8	35.3
		0.23	0.24	21	14	1.6	4.7	1.8	2.4
1000	3.81	0.24	0.38	1223	733	14	110	35.1	31.4
		0.24	0.25	44	28	1.7	5	2.9	2.8
1100	6.27	0.32	−0.23	1013	705	16.1	96	43	35.3
		0.16	0.13	15	10	1.1	3.9	1.9	2
1150	4.26	0.11	0.76	1950	1182	17.3	97.1	38.9	40
		0.24	0.25	43	30	1.7	5.6	2.3	3
1200	4.91	0.81	0.9	7070	3771	18	93.1	51.4	54.5
		0.28	0.27	170	81	1.2	4.2	3	2.3
1250	3.96	1.08	0.45	9470	4920	19.3	123.1	52.2	50.1
		0.36	0.27	170	110	1.5	6.3	3.2	3.2
1300	15.23	0.39	0.78	12830	6660	19.1	110.5	50.5	49.2
		0.13	0.13	130	71	1	2.5	1.5	1.1
1350	46.84	0.29	0.35	13470	7072	19.8	94.1	62.8	67.9
		0.06	0.06	100	50	0.5	1.4	1	0.8
1400	1.2	0.48	0.39	5740	2980	20.1	79.9	61.06	69.2
		0.5	0.39	260	150	2.6	5.6	3.6	3.6

Table 2. *Continued*. Raw I-Xe data for the Shallowater standard and Campo del Cielo silicates.

T, °C	$^{132}Xe \times 10^{-12}$. cm^3 STP g^{-1}	$^{132}Xe \equiv 100$							
		^{124}Xe	^{126}Xe	^{128}Xe	^{129}Xe	^{130}Xe	^{131}Xe	^{134}Xe	^{136}Xe
1450	0.99	0.89	0.37	1271	725	15.8	76.5	46.3	40.3
		0.94	0.43	73	46	3.6	10	7	5.6
1500	0.83	−0.05	−0.66	961	600	16.6	103.4	55	40.3
		0.58	0.78	52	30	1.9	6.8	5.8	5.8
1600	1.59	0.08	−0.28	429	317	12	83.2	41.6	26.6
		0.38	0.27	19	17	2.2	5.7	3.8	2.4
1700	9.29	0.4	0.27	967	606	14.8	78.9	42.78	37.2
		0.1	0.16	14	10	1	1.9	1.8	1.8
1800	19.21	0.48	0.35	8.89	101.3	16.1	80.9	40.1	34.1
		0.12	0.1	0.6	2.4	0.9	2.6	1.4	1.2
Total	132.51	0.4	0.39	7253	3827	17.8	98.9	50.7	50.2
		0.04	0.04	52	26	0.3	0.9	0.5	0.41
900	11.76	−0.05	−0.53	375	144	11.8	124	29.9	40.3
		0.49	0.67	23	14	2.7	12	5.7	4.5
1000	10.89	−0.08	0.28	108	118	18.1	115	32.2	25.4
		0.67	0.61	10	10	3.2	10	5	3.3
1100	12.8	1.41	0.49	359	274	15.5	211	36.9	32
		0.52	0.56	21	15	3.4	12	6.3	3.8
1200	11.37	−0.08	0.29	1947	1161	12.7	405	44.2	40.9
		0.5	0.56	58	43	2.5	23	23.1	4.6
1250	9.97	1.22	1.28	1990	1225	9.7	581	49.7	41.6
		0.66	0.63	120	81	3.1	51	6.6	6.5
1300	8.92	−0.84	−0.25	2125	1246	20	894	42.3	53.9
		0.55	0.91	97	65	3.3	68	4.3	6.7
1350	7.1	−1.00	−0.01	911	606	19	465	34.5	52.4
		1.04	0.81	53	30	3.7	26	7.6	7.1
1400	8.64	−0.27	−0.91	808	580	17.17	434	33.4	27.7
		0.66	0.69	38	30	2.7	34	9	4.2
1500	9.72	0.41	0.58	580	410	18.17	471	41.4	32.6
		0.46	0.65	29	20	3.67	28	5	5
1600	9.77	−0.10	−0.15	656	462	15.3	489	45.4	33.2
		0.53	0.62	31	21	2.2	24	4.4	5.7
Total	100.9	0.14	0.13	957	603	15.5	398	38.9	37.4
		0.19	0.21	24	16	1	11	1.8	1.6

Activation energies for $^{129*}Xe$ diffusion during stepwise analyses of diopside and oligoclase can be estimated from correlations in the Arrhenius diagrams of Fig. 4, where ln (D/a^2) is plotted versus the inverse extraction temperature, with D being the diffusion coefficient and a being the effective radius for diffusion (Dodson 1973).

We calculated the diffusivities D/a^2 from the release rate of $^{129*}Xe$, f, as a function of extraction temperature T for both Campo del Cielo silicates studied here (Fechtig and Kalbitzer 1966):

$$\frac{D_{i+1}}{a^2} = \frac{\left(f_{i+1}^2 - f_i^2\right) \cdot \pi}{36 \cdot \Delta T_{i+1}} \qquad (f < 10\%) \tag{1}$$

$$\frac{D_{i+1}}{a^2} = \frac{1}{\pi^2 \cdot \Delta T_{i+1}} \left[-\frac{\pi^2}{3}(f_{i+1} - f_1) - 2\pi \left(\sqrt{1 - \frac{\pi}{3} f_{i+1}} - \sqrt{1 - \frac{\pi}{3} f_i} \right) \right] \qquad (10 < f < 90\%) \tag{2}$$

$$\frac{D_{i+1}}{a^2} = \frac{1}{\pi^2 \cdot \Delta T_{i+1}} \ln \left(\frac{1 - f_i}{1 - f_{i+1}} \right) \qquad (f > 90\%) \tag{3}$$

The Arrhenius plot for diopside, shown in Fig. 4, is defined by the 1150–1350 °C extraction points approaching the major release peak at about 1400 °C. The corresponding activation energy for the diffusion of radiogenic $^{129*}Xe$ is about 201 kcal mole^{-1}. The

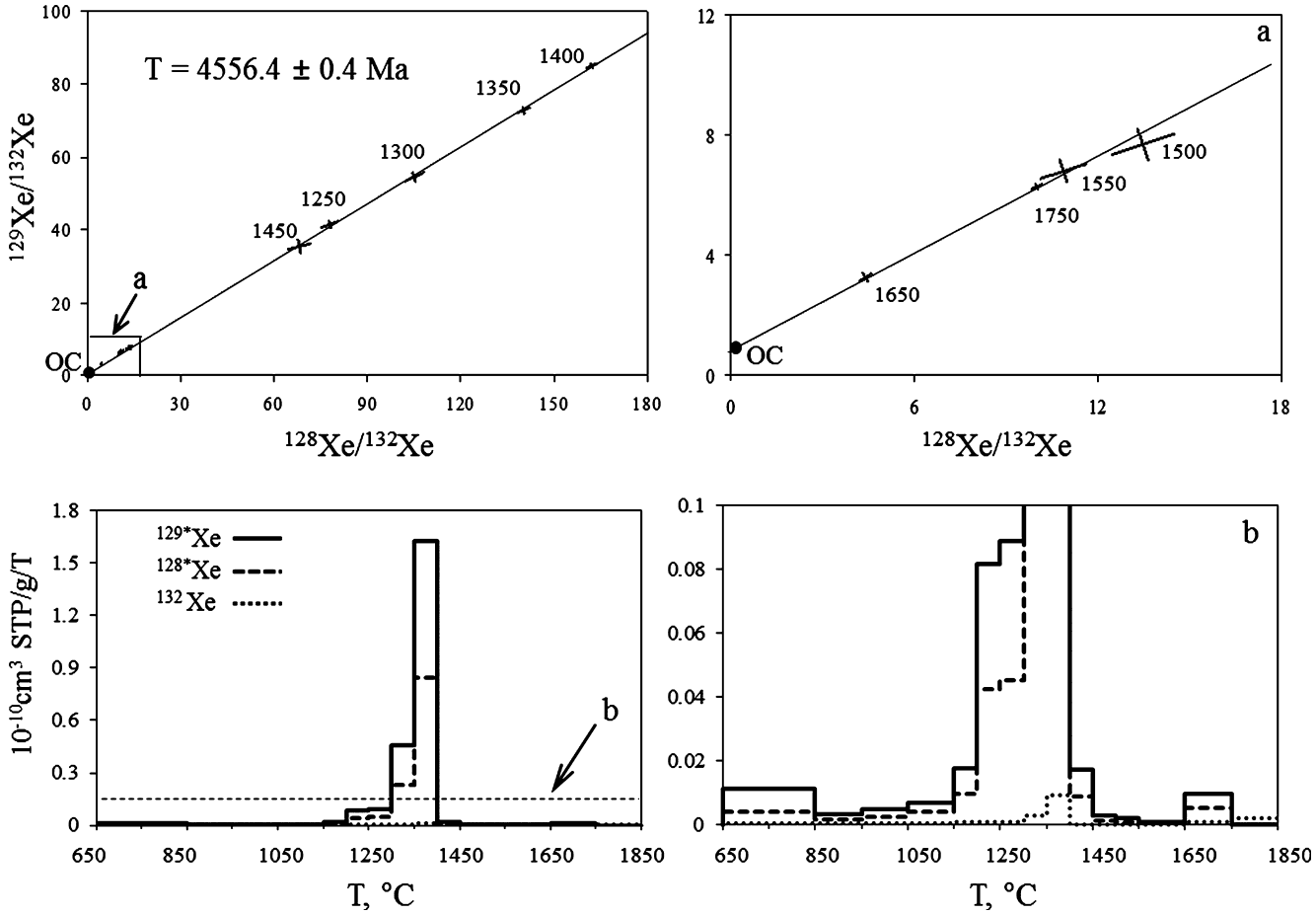

Fig. 2. I-Xe isochron and release profiles of the radiogenic $^{128*}Xe$ and $^{129*}Xe$ as a function of temperature for a diopside grain separated from the Campo del Cielo inclusion. The slope of the correlation line is 0.5173 ± 0.0038; $^{129}Xe/^{132}Xe$ = 1.03 at the OC $^{128}Xe/^{132}Xe$ value (0.083). The I-Xe age of diopside is calculated relative to Shallowater. The slope of the Shallowater correlation line is 0.6686 ± 0.0036, $^{128*}Xe/^{129*}Xe$ = 1.75, the isotopic composition of the trapped component is consistent with OC value.

Arrhenius plot for oligoclase (Fig. 4) is defined by 5 extraction points in the 1050–1350 °C temperature range; the corresponding activation energy for $^{129*}Xe$ is about 171 kcal mole^{-1}. As each experimental step is about 50 °C, the 1350 °C extraction step for oligoclase includes gas released in the 1300–1350 °C interval up to the melting of oligoclase at 1350 °C. If this last extraction step is not taken into account, the activation energy for oligoclase will be higher than the one given above, but still lower than the one for diopside. What is important here is the difference in activation energies. Calculated here under the same experimental conditions for two different silicates, the activation energies indicate that diopside is indeed more retentive than oligoclase. Both values are in agreement with earlier data for a silicate inclusion of complex chemical composition separated from the IAB iron meteorite Caddo County (189 kcal mole^{-1}, Bogard et al. 2005). The activation energy for the diffusion of ^{128}Xe from the IAB iron meteorite EET 83333 was reported to be about 82 kcal mole^{-1}, but the sample consisted of approximately 50% silicate clear/amber grains and approximately 50% opaque material (possibly troilite; Bogard et al. 2005).

The absolute ages of the diopside and plagioclase inclusions, 4556.4 ± 0.4 and 4558.0 ± 0.7 Ma, respectively, are in good general agreement with previously reported I-Xe ages for silicates from IAB iron meteorites (Podosek 1970; Niemeyer 1979a; Takeda et al. 2000; Bogard et al. 2005). However, these new I-Xe ages are much better defined as each datum is unique, referring to the age of a single silicate crystal of known chemical composition. All of the previous measurements were carried out on silicates, which had been crushed and chemically treated to remove the metal. Those samples were, consequently, mixtures of grains of different types of silicates (olivine, pyroxene, diopside, and plagioclase are all abundantly present in IAB irons), so the resulting I-Xe ages correspond to some kind of average closure time of these different minerals.

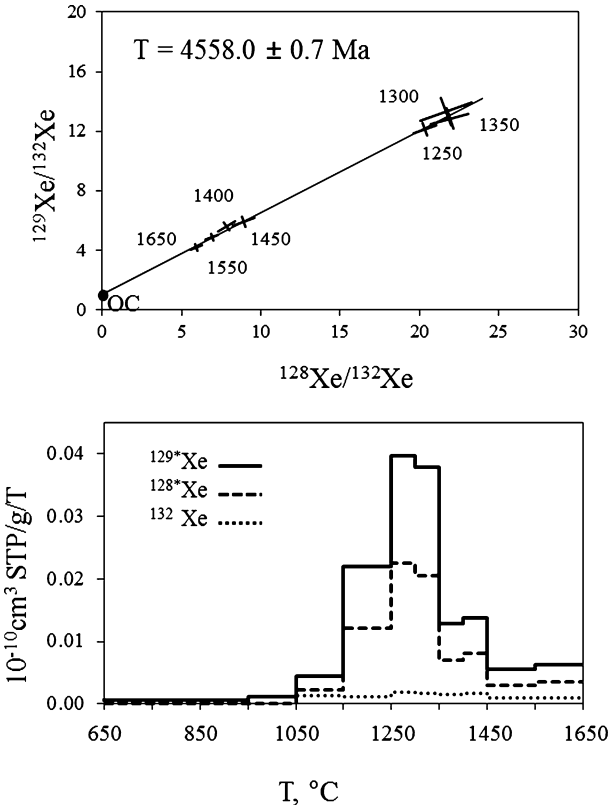

Fig. 3. I-Xe isochron and release profiles of radiogenic $^{128*}Xe$ and $^{129*}Xe$ as a function of temperature for an oligoclase grain separated from the Campo del Cielo inclusion. The slope of the free fit correlation line is 0.5547 ± 0.0153; $^{129}Xe/^{132}Xe = 1.07$ at the OC $^{128}Xe/^{132}Xe$ value (0.083). The I-Xe age of oligoclase is calculated relative to Shallowater. The slope of the Shallowater correlation line is 0.6686 ± 0.0036, $^{128*}Xe/^{129*}Xe = 1.75$, the isotopic composition of the trapped component is consistent with OC value.

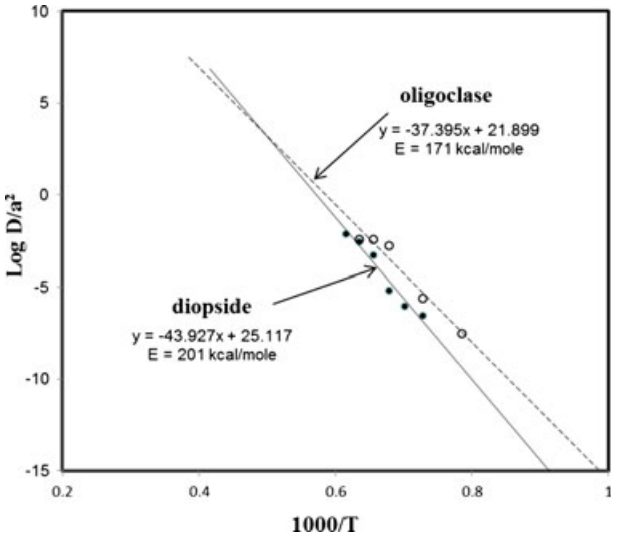

Fig. 4. Arrhenius plot, log D/a^2 versus $1000/T$, for radiogenic $^{129*}Xe$ from the Campo del Cielo 1AB meteorite. Diopside (filled circles) and oligoclase (open circles) grains from these inclusions define distinct linear trends with activation energies of ~201 and ~171 kcal $mole^{-1}$, respectively.

To investigate how an admixture of oligoclase would affect the I-Xe age of the diopside grain studied here, we considered mixtures of these two silicates with incrementally increasing contributions from oligoclase. The concentrations of radiogenic $^{129*}Xe$ and $^{128*}Xe$ in Campo del Cielo diopside are about one order of magnitude higher than in oligoclase; as a result, a 90% pure oligoclase separate (by weight) would account for only 50% of all released radiogenic Xe, the remaining 50% coming from a small 10% admixture of diopside. Although the release profiles for $^{128*}Xe$ and $^{129*}Xe$ in diopside and oligoclase overlap, they are significantly different. In diopside, 70% of $^{129*}Xe$ was released in a single 1350–1400 °C temperature step. With the highest radiogenic/trapped Xe ratio in this extraction, the corresponding data point lies farthest from the OC trapped component on a three-isotope plot, effectively defining the slope of the apparent isochron of the modeled mixture. When the contribution of oligoclase xenon in this diopside/oligoclase model increases, the slope of the line on the three isotope plot also gradually increases until this mixture is dominated by oligoclase and the corresponding correlation line on the three-isotope plot is then identical to the oligoclase isochron. In our case, mixing of these two xenon carrier phases results in seemingly well-defined correlation lines and apparent I-Xe ages. The resulting apparent isochron, for a 90% oligoclase/10% diopside sample mixture based upon the silicates studied here, corresponds to an age intermediate to I-Xe ages of pure diopside and pure oligoclase (Fig. 5), but reflects the closure time of neither pure mineral.

DISCUSSION

It is evident from the X-ray spectra of these two silicates, from release profiles of radiogenic $^{128*}Xe$ and $^{129*}Xe$, and from activation energies and diffusion properties that these two minerals are indeed distinct silicates, diopside and oligoclase, with different crystallization temperatures, and different closure temperatures. Diopside is the more refractory of the two; thus, its I-Xe age should be older, reflecting the thermal history of diopside and the earlier closure of the I-Xe system in that mineral. But, this is not the case. In fact, diopside is 1.6 ± 0.6 Ma younger than the oligoclase. How is it possible that these two silicate inclusions, separated only by 9 mm of metal, have I-Xe ages that contradict their thermal properties? First, as 1.6 Ma is not a large time difference, we must examine

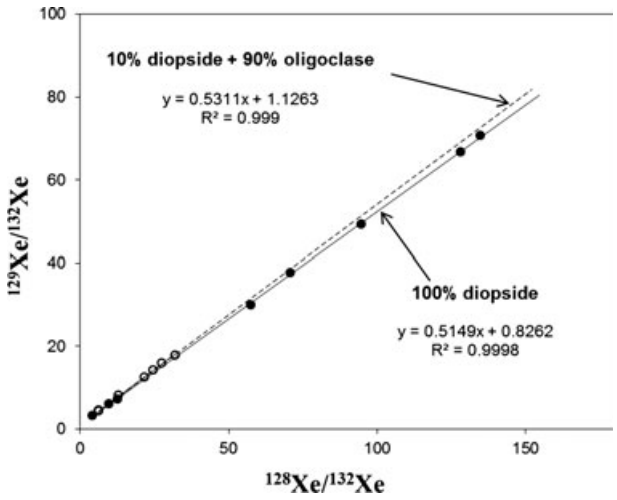

Fig. 5. An apparent I-Xe isochron for a hypothetical diopside–oligoclase mixture (10–90% by weight) shown in comparison with the isochron for the diopside grain studied here. Xe isotopic compositions for the diopside–oligoclase sample extraction steps were calculated based on the oligoclase extraction temperature intervals.

the possibilities of some systematic bias or error and finally ask the question "is it real"?

This difference in age cannot be due to variations in neutron fluence during irradiation. We take precautions to minimize any fluence variations by active placement geometry and verify what we have done by proper monitoring. For horizontal control, the irradiation package was continuously rotated, with the fluence monitored by neutron flux wires placed in the middle of the capsule and around the perimeter where the sample vials are located. For vertical control, we place the samples at the peak of the pool neutron flux, where any variation with vertical position is minimal. We observe a maximum neutron fluence variation of 1–2% for a 2 cm distance from the flux peak where the samples are located. Our samples all reside within a few mm from this peak where the flux gradient is negligible. Thus, we believe that the neutron fluence each sample received is the same to probably 0.1% (for reference, a 2% fluence variation corresponds to an apparent age difference of 0.4 Ma; a 0.1% uncertainty in fluence corresponds roughly to a 0.01 Ma age uncertainty). The 1.6 ± 0.6 Ma relative age difference of the two minerals studied here seems rather small, but this precision is routinely and reproducibly achieved in I-Xe dating (Hohenberg and Pravdivtseva 2008).

Wlotzka and Jarosewich (1977) analyzed 19 sections from 9 different inclusions of the El Taco fragment of Campo del Cielo and observed distinct differences in the mean FeO content among the different inclusions, which could not be explained by nonrepresentative sampling. Disequilibrium was also apparent between olivine and pyroxene in a given inclusion and it was even observed in single olivine and pyroxene grains. The rims of olivine, pyroxene, and diopside grains had lower iron contents than the central parts, the opposite of what crystallization zoning should produce. Wlotzka and Jarosewich (1977) argued that, if precursor material for Campo del Cielo silicates is chondritic, it could be reconstructed by the addition or subtraction of small amounts of diopside and/or plagioclase of analyzed composition, and demonstrated that it can be matched quite well for all inclusions studied by them. They suggested partial melting and redistribution of the melt as the mechanism responsible for these variations in mineralogical composition. In this case, oligoclase and diopside would be the first minerals to melt at 1180 °C and 1395 °C, respectively. What is intriguing here is that the different inclusions required different corrections to match the initial chondritic composition, and that diopside and plagioclase were not lost in proportional amounts. Highly variable amounts of metal, troilite, and graphite in these silicate inclusions lead to the conclusion that some of the metal, some of the troilite, and most of the graphite are probably secondary and were introduced into the silicate inclusions later (Wlotzka and Jarosewich 1977). Large ^{182}W excesses in silicates from Campo del Cielo also point to the disequilibrium between matrix and silicate inclusions in this meteorite (Schulz et al. 2006). The identical tungsten isotopic composition of matrix and inclusion metal indicates that the inclusion metal is derived from matrix metal and is unrelated to the host phase of tungsten in the silicate inclusions.

The polished section from the Campo del Cielo inclusion studied here is rich in diopside and oligoclase, which seem to be missing from some of the silicate-rich inclusions from the same meteorite (Wlotzka and Jarosewich 1977). It is clear that the diopside and oligoclase grains analyzed here could not have formed at the present locations, which are just 9 mm apart. Any secondary event capable of resetting the I-Xe system would have affected the less refractory oligoclase first, resulting in partial loss of radiogenic ^{129*}Xe (disturbed isochron and/or a younger I-Xe age). Or, if the temperature was high enough for both oligoclase and diopside to melt, diopside would be the first to crystalize as the impact site cooled below 1390 °C, resulting in an older I-Xe age. In order for the I-Xe system in the oligoclase grain to close earlier, it had to cool from 1360 to 1160 °C *before* the exsolution of diopside at the higher temperature of 1390 °C. The only way for the I-Xe system in oligoclase to close 1.6 ± 0.6 Ma earlier than in diopside is if these two silicates formed at different locations, presumably as the result of separate impact-produced heating events. If the target asteroid is highly

porous (Wasson 1991), the projectile may penetrate relatively deep, and much of the energy may be retained under an insulating regolith. Compression of the asteroid material caused by the impact will allow for a more efficient conversion of the kinetic energy to heat, as it is an adiabatic process, resulting in the melting of oligoclase and/or diopside near the impact site. Such multiple impacts and subsequent redistribution of the impact-produced melt could be responsible for the variations in plagioclase and diopside losses observed by Wlotzka and Jarosewich (1977). They could also be responsible for the 1.6 ± 0.6 Ma difference in the closure times of the I-Xe system in diopside and oligoclase that we observe here. In this case, each I-Xe age would have survived reassembly and corresponds to the Xe closure time of the mineral at a different location on the IAB parent body.

The question remains of how these two silicate grains ended up so close together in one Campo del Cielo inclusion surrounded by graphite rims, and separated by metal. Benedix et al. (2000) proposed a collisional fragmentation and gravitational reassembly scenario to explain the mixture of solid silicate rock fragments with molten metallic Fe,Ni–FeS in the IAB parent body. The presence of angular chondritic silicates in several IAB irons (Campo del Cielo, Landers, Lueders, Pine River, among others) is perhaps better explained if they formed by mixing after the impact. In this case, the cooler chondritic silicates mix into metallic melt, causing rapid cooling and solidification of the molten metal (Benedix et al. 2000). Based on the small sizes of the γ–iron crystals parental to the Widmanstätten pattern and the limited thermal effects recorded in the silicates, Wasson and Kallemeyn (2002) also argued for a high cooling rate through the γ–iron stability field. They proposed that the impact-induced melt was initially hotter than the combined mix of silicates and metal in the local region, and the melt cooled rapidly by heat conduction into the cooler surroundings, mainly the silicates. According to Wasson and Kallemeyn (2002), such independent impact-induced melting events could be responsible for the close compositional relationships between different sets of IAB irons, and could explain some features of these differentiated meteorites. Nevertheless, they cannot explain the situation observed in Campo del Cielo, in which the degree of loss of a low-temperature plagioclase-rich melt is highly variable on a scale of centimeters (Wlotzka and Jarosewich 1977).

We suggest that these silicates were formed in different locations remote to their present location and perhaps at different depths within the IAB parent body in separate events triggered by impacts on a porous chondritic asteroid (Scott 2004). Such impacts can produce local heating and melting of less refractory silicates, leading to removal of the melt and recrystallization of diopside and oligoclase. It is hard to imagine that impacts by projectiles of various sizes and speeds would result in impact melt pools of identical size and temperature and in target material of similar chemical composition. The outcome of different impacts would have to be very different. This could explain variations in diopside and plagioclase losses from Campo del Cielo inclusions observed by Wlotzka and Jarosewich (1977). If so, the unique I-Xe ages of diopside and oligoclase would reflect the time of these impacts, although the exact relationship between impact and closure times would depend upon the location of the crystallization sites. Later, a larger scale catastrophic collision of the type proposed by Benedix et al. (2000, 2005) may have caused breakup and reassembly of the debris and brought diopside and oligoclase within 9 mm of each other. The metal melt cooled rapidly and most probably was less than 1250 °C when it surrounded the silicate inclusions studied here, resulting in small sizes of γ–iron crystals. This later catastrophic event apparently did not reset the I-Xe systems in diopside and oligoclase studied by us, which still reflect the original closures at their respective remote sites. The closure time of the I-Xe system in diopside sets a time limit for this impact-related heating and reassembly event. It must have occurred later than 4556.4 ± 0.4 Ma, the age of the diopside grain and the younger of two minerals studied here, about 11 Ma after formation of CAIs (Amelin et al. 2002, 2010; Connelly et al. 2012).

Acknowledgments—We thank Dr. Tim Swindle and Dr. Jamie Gilmour for their critical and constructive reviews and Dr. Ingo Leya for helpful suggestions and editing. The Campo del Cielo sample was provided by Harald Stehlik. This work was supported by NASA grant #NNG06GE84G and FWF (Austria).

Editorial Handling—Dr. Ingo Leya

REFERENCES

Alexander E. C. Jr. and Manuel O. K. 1968. Xenon in the inclusions of Canyon Diablo and Toluca iron meteorites. *Earth and Planetary Science Letters* 4:113–117.

Alexander E. C. Jr., Srinivasan B., and Manuel O. K. 1969. Iodine-xenon dating of silicates from Toluca iron. *Earth and Planetary Science Letters* 6:355–358.

Amelin Y., Krot A. N., Hutcheon I. D., and Ulyanov A. A. 2002. Lead isotopic ages of chondrules and calcium-aluminum-rich inclusions. *Science* 297:1678–1683.

Amelin Y., Kaltenbach A., Iizuka T., Stirling C. H., Ireland T. R., Petaev M., and Jacobsen S. B. 2010. U-Pb chronology of the solar system oldest solids with variable $^{238}U/^{235}U$. *Earth and Planetary Science Letters* 300:343–350.

Benedix G. K., McCoy T. J., Keil K., and Love S. G. 2000. A petrologic study of the IAB iron meteorites: Constraints on the formation of the IAB-winonaite parent body. *Meteoritics & Planetary Science* 35:1127–1141.

Benedix G. K., Lauretta D. S., and McCoy T. J. 2005. Thermodynamic constraints on the formation conditions of winonaites and silicate-bearing IAB irons. *Geochimica et Cosmochimica Acta* 69:5123–5131.

Bogard D. D., Garrison D. H., and Takeda H. 2005. Ar-Ar and I-Xe ages and the thermal history of IAB meteorites. *Meteoritics & Planetary Science* 40:207–224.

Choy B., Ouyang X., and Wasson J. T. 1995. Classification and origin of IAB and IIICD iron meteorites. *Geochimica et Cosmochimica Acta* 59:593–612.

Connelly J. N., Bizzarro M., Krot A. N., Nordlund Å., Wielandt D., and Ivanova M. A. 2012. *Science* 338:651–655.

Dodson M. H. 1973. Closure temperature in cooling geochronological and petrological systems. *Contributions to Mineralogy and Petrology* 40:259–274.

Fechtig H. and Kalbitzer S. 1966. The diffusion of argon in potassium-bearing solids. In *Potassium argon dating*, edited by Schaeffer O. A. and Zahringer J. Berlin: Springer. pp. 68–106.

Gilmour J. D., Crowther S. A., Busfield A., Holland G., and Whitby J. A. 2009. An I-Xe constraint on the age of the CB chondrites and a re-evaluation of the closure age of Shallowater enstatite. *Meteoritics & Planetary Science* 44:573–580.

Hintenberger H., Schultz L., and Weber H. 1968. Rare gases in the iron and in the inclusions of the Campo del Cielo meteorite, El Taco. *Meteorite research*, Proceedings of a Symposium held in Vienna, Austria, August 7–13. pp. 895–900.

Hohenberg C. M. 1980. High sensitivity pulse-counting mass-spectrometer system for noble gas analysis. *Review of Scientific Instruments* 51:1075–1082.

Hohenberg C. M. and Pravdivtseva O. V. 2008. I-Xe dating: From adolescence to maturity. *Chemie der Erde* 68:339–351.

Hohenberg C. M., Hudson B., Kennedy B. M., and Podosek F. A. 1981. Noble gas retention chronologies for the St. Severin meteorite. *Geochimica et Cosmochimica Acta* 45:535–546.

Kelly K. R. and Larimer J. W. 1977. Chemical fractionations in meteorites-VIII: Iron meteorites and the cosmochemical history of the metal phase. *Geochimica et Cosmochimica Acta* 41:93–111.

Kracher A. 1982. Crystallization of a S-saturated Fe, Ni-melt, and the origin of iron meteorite groups IAB and IIICD. *Geophysical Research Letters* 9:412–415.

Kracher A. 1985. The evolution of partially differentiated planetesimals: Evidence from iron meteorite groups IAB and IIICD (abstract). 15th Lunar and Planetary Science Conference. p. C689.

Lodders K. and Fegley B. Jr. 1998. *The planetary scientist companion*. New York: Oxford University Press.

Maruoka T., Matsuda J., and Kurat G. 2001. Abundance and isotopic composition of noble gases in metal and graphite of the Bohumilitz IAB iron meteorite. *Meteoritics & Planetary Science* 36:597–609.

Mathew K. J. and Begemann F. 1995. Isotopic composition of xenon and krypton in silicate-graphite inclusions of the El Taco, Campo del Cielo, IAB iron meteorite. *Geochimica et Cosmochimica Acta* 59:4729–4746.

Matsuda J., Namba M., Maruoka T., Matsumoto T., and Kurat G. 2005. Primordial noble gases in a graphite-metal inclusion from the Canyon Diablo IAB iron meteorite and their implications. *Meteoritics & Planetary Science* 40:431–443.

Niemeyer S. 1979a. I-Xe dating of silicate and troilite from IAB meteorites. *Geochimica et Cosmochimica Acta* 43:843–860.

Niemeyer S. 1979b. ^{40}Ar-^{39}Ar dating of inclusions from IAB iron meteorites. *Geochimica et Cosmochimica Acta* 43:1829–1840.

Norimasa O. 1990. Relationship between crystallization temperature and melting temperature in crystalline materials. *Journal of Material Science* 25:1623–1631.

Podosek F. A. 1970. Dating of meteorites by the high-temperature release of iodine-correlated ^{129}Xe. *Geochimica et Cosmochimica Acta* 34:341–366.

Pravdivtseva O. V., Meshik A. P., Hohenberg C. M., and Wasserburg G. J. 2000. I-Xe record of cooling in K-feldspar inclusion from Colomera (IIE) iron (abstract #1929). 31st Lunar and Planetary Science Conference. CD-ROM.

Pravdivtseva O. V., Meshik A. P., Hohenberg C. M., and Petaev M. 2009. Interpreting the I-Xe system in individual silicate grains from Toluca IAB. *Meteoritics & Planetary Science* 44:1787–1796.

Schulz T., Münker C., Mezger K., and Palme H. 2006. Age and origin of IAB iron meteorites and their silicate inclusions inferred from Hf/W chronometry (abstract #1401). 37th Lunar and Planetary Science Conference. CD-ROM.

Scott E. R. D. 2004. Meteoritic constraints on collisional rates in the primordial belt and its origin (abstract #1990). 35th Lunar and Planetary Science Conference. CD-ROM.

Takeda H., Bogard D. D., Mittlefehldt D. W., and Garrison D. H. 2000. Mineralogy, petrology, chemistry, and ^{39}Ar-^{40}Ar and exposure ages of the Caddo County IAB iron: Evidence for early partial melt segregation of a gabbro area rich in plagioclase-diopside. *Geochimica et Cosmochimica Acta* 64:1311–1327.

Vogel N. and Renne P. R. 2008. ^{40}Ar-^{39}Ar dating of plagioclase grain size separates from silicate inclusions in IAB iron meteorites and implications for the thermochronological evolution of the IAB parent body. *Geochimica et Cosmochimica Acta* 72:1231–1255.

Wasson J. T. 1991. Layered tektites: A multiple impact origin for the Australasian tektites. *Earth and Planetary Science Letters* 102:95–109.

Wasson J. T. and Kallemeyn G. W. 2002. The IAB iron-meteorite complex: A group, five subgroups, numerous grouplets, closely related, mainly formed by crystal segregation in rapidly cooling melts. *Geochimica et Cosmochimica Acta* 66:2445–2473.

Wasson J. T., Willis J., Wai C. M., and Kracher A. 1980. Origin of iron meteorite groups IAB and IIICD. *Zeitschrift für Naturforschung* 35a:781–795.

Wlotzka F. and Jarosewich E. 1977. Mineralogical and chemical compositions of silicate inclusions in the El Taco, Campo del Cielo, iron meteorite. *Smithsonian Contribution, Earth Sciences* 19:104–125.